Electronic structure and magnetic properties of dilute Cr alloys with transition-metal impurities

S. N. Mishra*
Department of Nuclear and Atomic Physics, Tata Institute of Fundamental Research, Homi Bhabha Road, Mumbai-400005, India
(Received 21 February 2008; revised manuscript received 8 May 2008; published 2 June 2008)

By using full-potential linearized augmented plane wave (FLAPW) method based on the density function theory (DFT), we have performed *ab initio* calculations of electronic structure and magnetic properties for dilute alloys of Cr with transition metals. Here, we present our results for the local magnetic properties of 3*d* (Sc–Ni) and 4*d* (Y–Pd) impurities in Cr, as well as changes in macroscopic properties such as total magnetization and specific heat of Cr alloys, arising from impurity-induced host perturbations. Results obtained for nonmagnetic local density of states is analyzed within Stoner model, and the condition for local moment formation is found to be satisfied only for Fe, Co, and Ni. For all other cases including Mn, the impurity moments are predicted to be induced by Cr host. Systematic trends for the impurity local moments and hyperfine fields in antiferromagnetic Cr host have been established. The trends show remarkable similarity with those observed in ferromagnetic Fe, Co, and Ni hosts. While the impurity moments for Sc, Ti, V, and Mn are found to be antiparallel with respect to the near neighbor Cr moment, self-consistent solutions for Fe, Co, and Ni show ferromagnetic coupling. For 4*d* impurities, except for Rh and Pd, the exchange interaction remain antiferromagnetic. The calculated changes of the total moment due to host perturbations show qualitative agreements with data from magnetization measurements. A detailed comparison is made for the impurity-induced changes in the total density of states at Fermi energy E_F and experimentally measured electronic specific heat of Cr alloys. The results presented in this work provide comprehensive and improved understanding of electronic and magnetic properties of dilute Cr alloys. They are also useful for a common understanding of local magnetic properties of transition metal impurities in ferromagnetic and antiferromagnetic hosts.

DOI: 10.1103/PhysRevB.77.224402 PACS number(s): 71.20.Be, 71.15.Mb, 75.20.Hr

I. INTRODUCTION

Chromium is one of the most interesting elements of the periodic table because of its unique magnetic properties. It shows incommensurate spin-density wave antiferromagnetic behavior with a Neel temperature T_N=311 K, originating from nesting properties of the Fermi surface.[1] It also undergoes an order-order transformation at 123 K with a change spin orientation and the magnetic wave vector. The magnetic wave vector has also been found to change dramatically by alloying with other elements resulting in a crossover over from incommensurate to commensurate antiferromagnetic structure.[2] Apart from many interesting physics issues related to magnetism, chromium alloys are also useful for shape-memory and high-temperature applications. As such, investigations of chromium alloys, especially their magnetic properties, continue to be a subject of intense experimental and theoretical studies. Over the years, extensive experimental data have been compiled on the magnetic behavior of Cr alloys with 3*d* and 4*d* elements. The results have revealed that the magnetic moment, as well as the transition temperature, either increase or decrease depending on type of impurity. While elements to the left of Cr in the periodic table decrease the magnetic moment and T_N, impurities to its right show the opposite effect. Compared to the experimental situation, very few theoretical studies on magnetic behavior of dilute Cr alloys with transition metals have been carried out. As far as we know, only two such investigations have been reported in literature. By using linear-muffin-tin-orbital (LMTO) method, Antropov *et al.*[3] have studied the local magnetic moments of 3*d* impurities (V to Ni) in Cr, showing large magnetic moments for Fe and Co. Recently, Hashemifar *et al.*[4] have reported the magnetic moment and hyperfine field of several impurities in Cr including Fe, Ru, Rh, and Pd. Due to insufficient data available for the local moments and hyperfine fields of transition metal impurities in Cr, systematic trends in their behavior across the 3*d* and 4*d* series of elements have not been established so far. Furthermore, no theoretical study has been reported for other physical properties of Cr alloys such as: (i) impurity induced host perturbations; (ii) global changes in density of states and alloy magnetism; (iii) changes in electronic specific heat for which extensive experimental data are available in literature.

In this paper we present detailed *ab initio* calculations of electronic structure and magnetic properties of dilute Cr alloys with 3*d* (Sc–Ni) and 4*d* (Y–Pd) elements using full-potential linearized augmented plane wave (FLAPW) method within density functional theory (DFT). We calculate both the local magnetic properties of 3*d* and 4*d* impurity atoms in Cr, including hyperfine fields, as well as the changes in global properties arising from induced host perturbations. Our results for the nonmagnetic local density of states (LDOS) analyzed within Stoner model reveal that the condition for local moment formation is satisfied only for Fe, Co, and Ni. For all other cases, including Mn, the magnetic moments are predicted to be induced by Cr-host magnetism. The local magnetic moments and hyperfine fields of 3*d* and 4*d* impurities in antiferromagnetic Cr show systematic trends, which are remarkably similar to those reported in ferromagnetic hosts Fe, Co, and Ni. The calculated changes of the total moment due to impurity induced host perturbation agree with the data reported from magnetization measurements. Furthermore, results obtained for the changes of the total density of states at the Fermi energy agree well with specific heat measurements. The results presented in this

work provide comprehensive and improved understanding of electronic and magnetic properties of dilute Cr alloys. They are also useful for a common understanding of local magnetic properties of transition metal impurities in ferromagnetic and antiferromagnetic hosts.

II. CALCULATION DETAILS

The calculations presented in this paper have been performed within the framework of density functional theory[5,6] using the all-electron full-potential linearized augmented plane wave method as implemented in the WIEN2K package.[7,8] To achieve the representative condition of sufficiently dilute Cr-X alloys, a cubic supercell consisting of 27 bcc chromium unit cells, having 54 atoms was constructed by repeating the unit cell three times in x, y, and z directions ($3\times3\times3$). The Cr atom at the origin (0, 0, 0) of the supercell was replaced by the impurity atom. The unit cell thus constructed represents a Cr-X alloy of composition $Cr_{0.9815}X_{0.0185}$. In such a unit cell there are 8 nonequivalent atoms with lattice positions: Cr0/X (0, 0, 0), Cr1(1/6, 1/6, 1/6), Cr2(1/3, 0, 0), Cr3(1/3, 1/3, 0), Cr4(1/2, 1/6, 1/6), Cr5(1/3, 1/3, 1/3), Cr6(1/2, 1/2, 1/6), and Cr7/X (1/2, 1/2, 1/2). The labels for the Cr atoms are arranged according to their distance from the origin/impurity with Cr1 being the closest and Cr7 as the farthest. For the supercell used for our studies, the impurity atoms are well separated so that the impurity-impurity interaction can be considered to be small.

In the FLAPW method, the unit cell is divided into two regions: (i) nonoverlapping muffin-tin spheres of radius R_{MT} around each atom and (ii) the remaining interstitial region. For the wave functions inside the atomic spheres, a linear combination of radial function times spherical harmonics are used, while in the interstitial region a plane wave expansion is used. In our calculations, we have used R_{MT} values of 2.25 a.u. for Cr and 2.28–2.4 a.u. for the impurity atoms. The maximum multipolarity l of the wave functions inside the atomic sphere was restricted to $l_{\max}=10$. The wave functions in the interstitial region were expanded in plane waves with a cutoff of $k_{\max}=7.5/R_{\mathrm{MT}}^{\min}=3.33$ a.u.$^{-1}$. The charge density was Fourier expanded up to $G_{\max}=14\sqrt{Ry}$. For the exchange correlation potential, we used the Perdew–Burke–Ernzerhof formalism of the generalized gradient approximation (GGA).[9] For sampling of the Brillouin zone, a k-mesh with 35 special k-points in the irreducible zone was used. All calculations were performed using the equilibrium lattice parameters obtained by calculating the total energy at different volumes and fitting the results to Birch–Murnaghan equation of state[10] implemented within Wien2k program.[7] Due to lattice imperfection caused by the impurity, the atoms at their ideal positions experience nonzero force, which were minimized to less than 1 mRy/a.u by allowing the atoms to relax to new positions. For all of the cases studied here, calculations were performed with and without spin polarization, the later being useful for extracting information related to local moment formation on the impurity. For the spin polarized case, calculations were performed using the commensurate antiferromagnetic structure of Cr in which the magnetic moments for atoms 1, 4, 6, and 7 were considered to be parallel with respect to an arbitrarily defined magnetic field direction while, the moments of the atoms 0, 2, 3, and 5 were taken as being antiparallel. For the cases of Mn, Fe, Co, and Ni, calculations were also performed by flipping the impurity spin direction and the self-consistent ground state was determined by comparing the total energy of the two spin configurations.

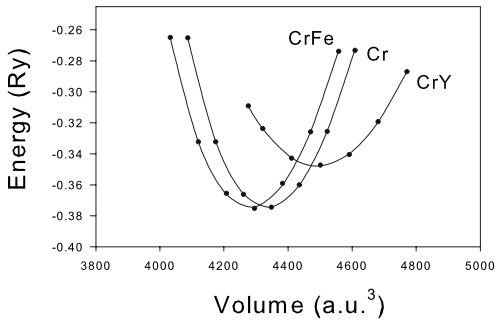

FIG. 1. Total energy as a function of unit cell volume for some representative cases of $Cr_{53}X$; X=Cr, Fe, and Y together with the fits (solid lines) to Birch—Murnaghan equation of state (see text). The energy axis has an arbitrary zero point.

III. RESULTS AND DISCUSSION

A. Structural properties

Figure 1 shows the variation of total energy E_{tot} at different volumes for a few representative cases: pure Cr, Cr-Fe, and Cr-Y. The calculated structural properties e.g., equilibrium lattice constants, near neighbor distances, cohesive energies defined as $E_c=E_{\mathrm{alloy}}-\Sigma E_{\mathrm{Atom}}$ with E_{tot} and E_{Atom} being the self-consistent total energy of the supercell and energies of isolated atoms, and the bulk moduli of Cr-X alloys (X=Sc–Ni and Y–Pd) are summarized in Table I. The bulk moduli were obtained by fitting the total energy of the supercell at different volumes to Birch–Murnaghan equation of state.[10] For pure Cr, our results closely agree with the values reported in literature.[4,11] In all of the cases studied, the lattice constant a(Å) was found to decrease with the atomic number of the impurity atom X, while the bulk modulus and the cohesive energy peaks near the middle of the $3d$ ($4d$) series, suggesting a lowering of bond strength on either ends.

B. Density of states and specific heat

Figures 2 display the impurity projected LDOS for $3d$ impurities in Cr obtained from unpolarized, as well as spin polarized calculations. The results for the $4d$ impurities are shown in Fig. 3. Let us first look at the LDOS results from the nonmagnetic (unpolarized) calculations. Starting with the case of pure Cr, the calculated LDOS exhibits the typical three-peak structure of bcc metals with the Fermi energy falling in a pseudogap separating the lower-lying bonding states from the higher antibonding ones. The calculated Fermi energy E_F and the density states at E_F for paramagnetic Cr come out to be 0.759 Ry and 0.697 states/eV-atom, respectively, which agree with the values reported in literature.[12] In the case of Cr-X alloys, the features observed in LDOS of the impurity atoms, although qualitatively simi-

TABLE I. Summary of calculated structural properties of Cr–X alloys with different $3d$ and $4d$ impurities X=Sc-Ni and Y–Pd. a: (Å) super cell equilibrium lattice constant; d_{nn}(Å): near neighbor distance; E_c(Ry): cohesive energy per unit of $Cr_{53}X$; and B(Gpa): Bulk modulus.

Impurity X	a	d_{nn}	E_c	B
Sc	8.673	2.504	−16.99	179
Ti	8.642	2.495	−17.18	183
V	8.623	2.489	−17.34	187
Cr	8.628	2.491	−17.65	190
Mn	8.609	2.485	−17.68	191
Fe	8.591	2.480	−17.36	187
Co	8.583	2.478	−17.27	185
Ni	8.595	2.482	−17.06	181
Y	8.731	2.521	−17.08	178
Zr	8.694	2.510	−17.46	188
Nb	8.672	2.504	−17.51	191
Mo	8.668	2.502	−17.68	198
Tc	8.646	2.496	−17.61	196
Ru	8.632	2.492	−17.53	191
Rh	8.633	2.492	−17.34	184
Pd	8.648	2.496	−16.96	172

lar to Cr, one can easily notice impurity-dependent differences with respect to the positions of the bonding and antibonding states relative to E_F. While the centroid of the bonding states does not show much change, the position of the antibonding peak varies with the impurity atomic number Z_{imp}. Beginning with X=Sc, with increasing Z_{imp}, the antibonding peak progressively moves to closer to E_F. For the heavier impurities Mn, Fe, Co, and Ni the antibonding states appear as a sharp resonance—virtual bound state (VBS)—passing through the E_F between Fe and Co. This leads to a large enhancement in the density of states at the Fermi energy $N(E_F)$, which was determined to be 1.2, 3.0, 2.6, and 1.7 states/eV-atom for Mn, Fe, Co, and Ni, respectively. For the early impurities the $N(E_F)$ value come out to be $\leq$0.6 states/eV-atom. The nonmagnetic calculations for Cr-X alloys with $4d$ impurities exhibiting similar features yield much smaller $N(E_F)$ values. Figure 4 shows the variation of $N(E_F)$ in Cr-X alloys with X=Sc-Ni and Y-Pd. By applying Stoner criteria:[13] $IN(E_F>)1$, one can find if the formation of local moment for $3d$, $4d$ impurities in Cr is possible or not. Here, I is the well-known Stoner exchange parameter. By using I=0.9 eV, 0.6 eV known for $3d$ and $4d$ impurities, respectively,[13,14] the critical value of $N(E_F)$ above which an intrinsic local moment on the impurity is likely to form in Cr matrix comes out to be 1.08 states/eV-atom for $3d$ and 1.67 states/eV-atom for $4d$ impurity atoms. By examining the results shown in Fig. 4, it can be seen that the Stoner condition for local moment formation in Cr host is satisfied for Fe, Co, and Ni, while in the case of Mn the $N(E_F)$ value falls close to the Stoner limit, which indicates that the magnetic moment of Mn in Cr is likely to be unstable. It should be mentioned here that the predicted moment instability for Mn in Cr is

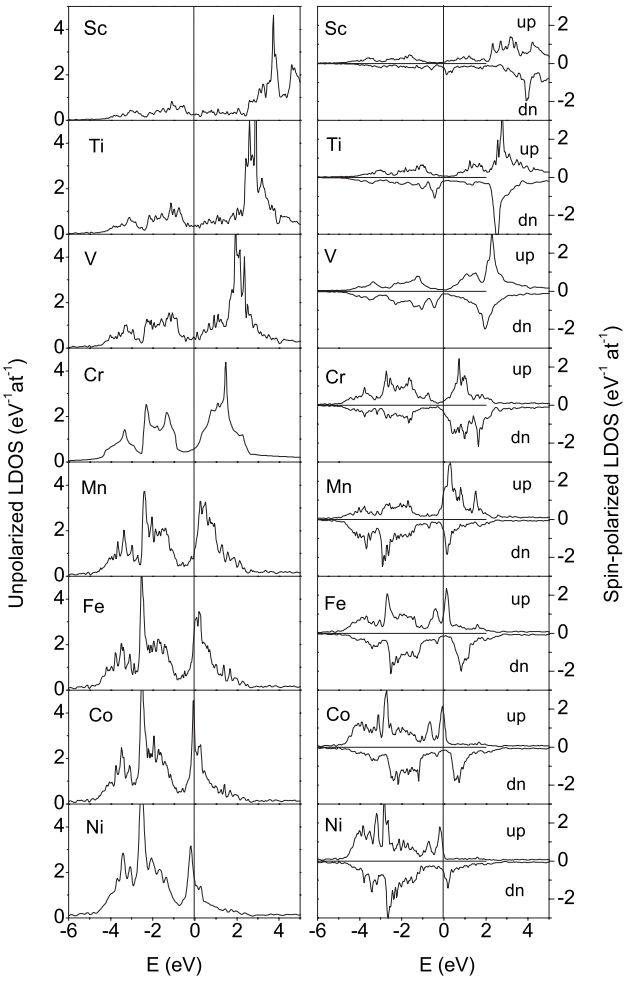

FIG. 2. Local density of states for $3d$ impurities in Cr. Panel on the left corresponds to unpolarized LDOS, while the right panel is for spin polarized cases. The Fermi energy E_F is shown as a vertical solid lines passing through zero of the energy axis.

born out in our spin-polarized calculations, where we observe two different stable solutions having similar total energies but opposite spin alignment. For all other cases studied here, the $N(E_F)$ falls below the critical value, which suggests that the moments of these impurities most likely are induced by the surrounding magnetic Cr atoms.

We now examine the results obtained from the spin-polarized calculations. Starting with pure Cr, the LDOS for the majority as well as the minority spin states exhibit the typical pseudogap structure yielding a magnetic moment of $1.19\mu_B$, which agrees with the values reported from earlier calculations.[4,11,15–17] The calculated moment of Cr, however, turns out to be higher than the experimental value reported from neutron diffraction measurements.[1] Cottenier *et al.*[11] have shown that the magnetic moment of Cr in the antiferromagnetic phase is sensitive to the exchange correlation potential used. While GGA calculations overestimates the magnetic moment with respect to the experimental value, LDA is unable to find a stable antiferromagnetic ground state for Cr.[15–17] We believe that this difference in the absolute value of Cr magnetic moment does not influence the main conclusion of this paper.

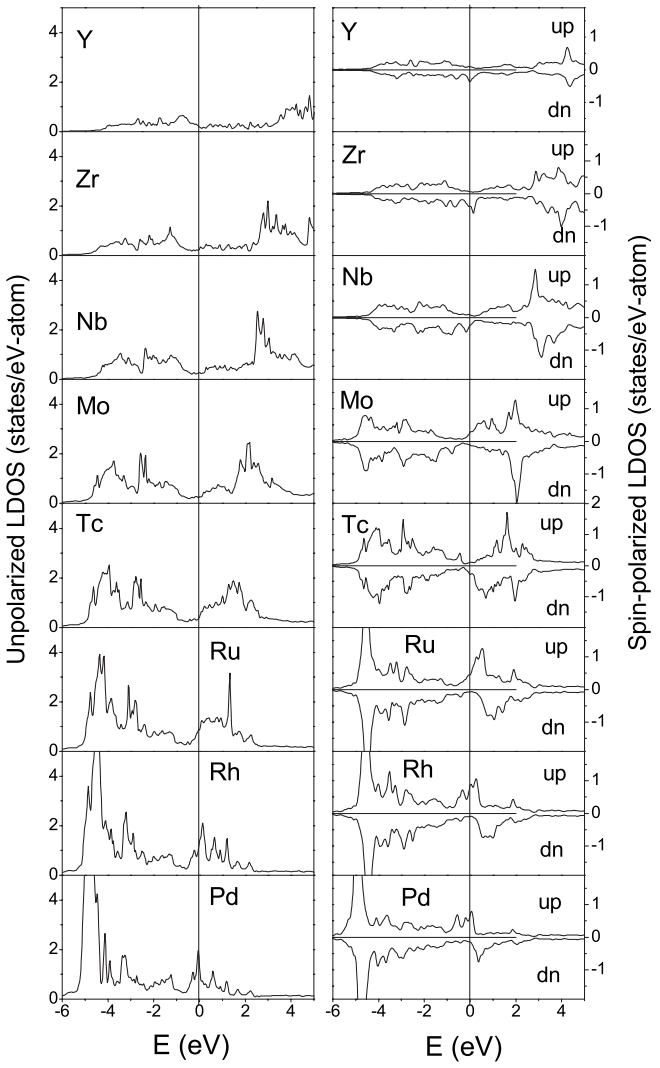

FIG. 3. Local density of states for 4*d* impurities in Cr. The left panel corresponds to unpolarized LDOS, and the right panel is for spin polarized cases. The vertical solid line through zero of the energy axis represents the position of the Fermi energy E_F.

Going to the Cr-*X* alloys, for the early impurities Sc, Ti, and V, the LDOS show the formation of unoccupied VBS for both the spin directions, which progressively moves closer to the Fermi energy with the increase in atomic charge. In the case of Mn, we find a sharp resonance—virtual bound state—in the minority-spin band just above E_F. In addition, a broader VBS is also seen in the majority-spin band at $\approx$0.4 eV above E_F. Moving further down in the series, the situation is different for Fe, Co, and Ni. Here, the VBS is visible in the majority-spin band, well separated from the unoccupied peak in the minority-spin band. The VBS in the majority-spin band passes through E_F between Fe and Co, consistent with the features observed in the nonmagnetic density of states (DOS) discussed above. The above feature reflects that the coupling between the moments of impurity and near neighbor Cr atoms changes sign between Mn and Fe. This is also manifested in the self-consistent moment values estimated by integrating the DOS below E_F. Going to the 4*d* elements, due to larger spatial extent of the 4*d* wave

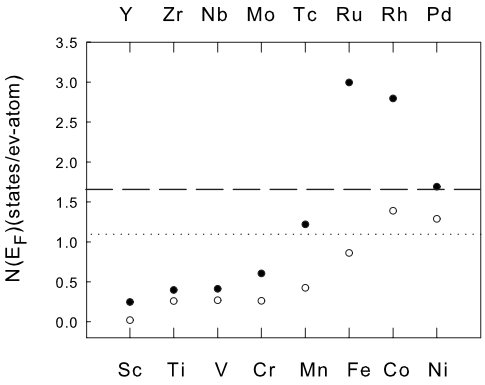

FIG. 4. Nonmagnetic local density of states at the Fermi energy for 3*d* and 4*d* impurities in Cr. The dotted and dashed lines represent the Stoner limits for local moment formation. 3*d*: Filled symbol and dotted line; 4*d*: open symbols and dashed line.

function and the resulting stronger hybridization with Cr valence states, the impurity states are broader compared to the 3*d* counterparts. The broader bands and the smaller exchange integral makes magnetism less favorable, consistent with Stoner analysis of the nonmagnetic DOS discussed above. Like the 3*d* cases—Fe, Co, and Ni— the LDOS of the late 4*d* impurities Ru, Rh, and Pd show the formation of VBS in the majority-spin band, crossing E_F near Ru-Rh. Here, it should be mentioned that for Mn we also find a stable solution with ferromagnetic coupling with slightly higher ($\approx$1 mRy) total energy compared to the ground state with antiferromagnetic coupling. This suggests that Mn in Cr is close to a magnetic instability, which is consistent with the prediction made from Stoner analysis of the unpolarized DOS results discussed above.

Next we discuss the total DOS at the Fermi energy for Cr-*X* alloys, which can provide information concerning thermodynamic properties, e.g., electronic specific-heat coefficient γ. As it is well known that electronic contribution to the specific heat is given by $C_e(T)=\gamma T$, where the coefficient γ is given by[18]

$$\gamma = (k_B^2\pi^2/3)n(E_F)(1+\lambda). \quad (1)$$

Here, $n(E_F)$ is the total DOS at the Fermi energy, k_B is the Boltzmann constant, and λ is the mass enhancement due to electron-phonon and/or electron-magnon interactions. For pure Cr, the calculated paramagnetic DOS, $n(E_F)=0.697$ states/eV-atom yields a γ value of 2.63 mJ-K^{-2} mol^{-1}. In the case of antiferromagnetic Cr, taking λ to be 0.25[19,20] the calculated $n(E_F)=0.323$ states/eV-atom leads to a γ value of $\approx$1.52 mJ-K^{-2} mol^{-1}. The γ values thus estimated for paramagnetic and antiferromagnetic Cr are close to the results reported in literature.[2,21–24] By differentiating the above equation, we obtain for the relative changes of γ, $n(E_F)$, and λ in the alloy:

$$\Delta\gamma/\gamma = \Delta n(E_F)/n(E_F) + \Delta\lambda/\lambda. \quad (2)$$

Since $\Delta\lambda$ is unknown, we compare in Fig. 7 the relative changes $\Delta n(E_F)/n(E_F)$ directly with the values $\Delta\gamma/\gamma$ measured experimentally. The $\Delta n(E_F)$ values shown in Fig. 7 have been calculated by summing the changes for the impu-

TABLE II. Summary of calculated magnetic properties of $Cr_{53}X$ (X=Sc-Ni and Y–Pd). M_0 (μ_B): Local magnetic moment of the impurity X; $\delta M_n(\mu_B)$: change in Cr magnetic moment for the seven near-neighbor shells around the impurity; and $\Delta M(\mu_B)$: change in net magnetic moment of the unit cell.

X	M_0	δM_1	δM_2	δM_3	δM_4	δM_5	δM_6	δM_7	ΔM
Sc	0.050	−0.126	+0.007	−0.035	+0.001	−0.021	−0.005	−0.012	−0.442
Ti	−0.158	−0.116	+.006	−0.029	+0.002	−0.019	−0.005	−0.01	−0.376
V	−0.704	−0.071	+0.009	−0.023	+.004	−0.012	+.002	−0.008	−0.348
Cr	−1.190	0	0	0	0	0	0	0	0.0
Mn	−1.466	+0.028	−0.018	+.012	−0.010	+0.005	−0.004	+0.001	0.433
Fe	0.217	−0.054	+0.008	−0.024	+0.001	−0.014	−0.004	−0.01	0.167
Co	0.901	0.011	−0.014	+0.005	−0.009	+.001	−0.005	−0.002	0.221
Ni	0.546	−0.025	−0.004	−0.012	−0.006	−0.010	−0.008	−0.009	0.067
Y	0.035	−0.136	+0.003	−0.036	−0.003	−0.021	−0.009	−0.012	−0.617
Zr	−0.084	−0.118	+.004	−0.035	−0.005	−0.017	−0.007	−0.010	−0.482
Nb	−0.244	−0.083	−0.002	−0.033	−0.007	−0.016	−0.009	−0.013	−0.405
Mo	−0.450	−0.056	+0.008	−0.020	+0.004	−0.006	0.00	−0.003	0.097
Tc	−0.417	−0.046	+0.005	−0.016	−0.001	−0.009	−0.004	−0.007	0.128
Ru	−0.226	−0.064	+0.012	−0.018	+0.006	−0.010	+0.001	−0.004	0.298
Rh	0.126	0.016	−0.038	−0.004	−0.021	−0.009	−0.016	−0.012	0.448
Pd	0.258	+0.043	−0.045	−0.007	−0.028	−0.015	−0.018	−0.013	0.345

rity cell and all Cr atoms in the seven shells around the impurity. Figure 7 clearly shows that the variation in the calculated changes in DOS qualitatively resembles the trend found in the experimentally measured $\Delta\gamma/\gamma$. As a noteworthy feature, we find that $3d$ impurities with ferromagnetic exchange coupling, e.g., Fe, Co, and Ni show large changes in $n(E_F)$ value, which are also reflected in the $\Delta\gamma/\gamma$ measurements. Considering the fact that Mn in Cr is close to ferromagnetic instability, as discussed above, we are tempted to believe that the large change in $\Delta n(E_F)/n(E_F)$ in this case is related to spin fluctuations arising from the magnetic instability.

C. Magnetic moments

The calculated magnetic moments for the $3d$ and $4d$ impurity atoms in Cr are summarized in Table II. Figure 5 shows the variation of impurity local moment across the $3d$ and $4d$ series elements. It can be noticed that $3d$ impurities such as V, Mn, Co, and Ni in Cr show large magnetic moments with magnitudes $-0.70\mu_B$, $-1.47\mu_B$, $0.90\mu_B$, and $0.55\mu_B$, respectively. On the other hand, the magnetic moment of Fe in Cr comes out to be rather small $\approx 0.22\mu_B$. Particularly noteworthy is the observation of a large magnetic moment for the nonmagnetic atom V, which is supported by the effective moment $\approx 1\mu_B$/V obtained from measurements of bulk magnetic susceptibility of dilute $Cr_{1-x}V_x$ alloys.[25] The calculated low magnetic moment of Fe in Cr is consistent with the results reported from Mössbauer and perturbed angular distribution studies,[26–28] but differ from the moment values $\mu_{Fe}=1.7-3.1\mu_B$ obtained from bulk susceptibility measurements.[2,29] Similarly, the calculated moment of Co impurities are lower compared to the values $\mu_{Co}=1.7-2.9\mu_B$ reported from macroscopic magnetization studies.[2] Theoretically, the magnetic behavior of $3d$ impurities in antiferromagnetic Cr host was earlier calculated by Antropov *et al.*[3] using linear muffin-tin orbital-atomic sphere approximation method. The moment values for V, Mn, Fe Co, and Ni were reported to be $0.36\mu_B$, $0.48\mu_B$, $\approx\pm 2\mu_B$, $-1.6\mu_B$, and $-0.13\mu_B$, respectively. Recently, using a 16-atom supercell—$Cr_{15}Fe$—and FLAPW method, Hashemifar *et al.*[4] calculated the magnetic moment of Fe to be $-0.61\mu_B$. They also reported an energetically close ferromagnetic solution with an Fe moment of $1.81\mu_B$. Our moment values significantly differ from these results, especially for Fe, Co, and Ni. We believe this difference is mainly due to the larger impurity concentrations corresponding to the smaller ($2\times 2\times 2$) supercell used in the previous calculations. Later, we shall illustrate the concentration dependence by comparing results obtained from our calculations made for a few cases of $Cr_{0.9815}X_{0.0185}$ ($3\times 3\times 3$ supercell with 54 atoms) and $Cr_{0.9375}X_{0.0625}$ ($2\times 2\times 2$ supercell with 16 atoms). The trends observed for the $3d$ impurity moments in antiferromagnetic Cr are qualitatively similar to those reported for ferromagnetic hosts Fe, Co, and Ni.[18,30–37]

The impurity atoms also results in a strong perturbation of the host Cr magnetic moments. The calculated moment change δM_n ($n=1,2,\ldots 7$) for Cr atoms in the first seven near neighbor shells around the impurities are listed in Table II. With increasing distance from the impurity site, the δM values decrease and show the typical Friedel-like oscillation. By summing the δM values for all of the atoms in unit cell, including the impurity shell, one can obtain the net change in magnetization $\Delta M=\delta M-M_{imp}+M_{Cr}$. Taking the impurity concentration to be $x=0.0185$ for the $3\times 3\times 3$ supercell, the calculated change in magnetization per impurity atom for the Cr-X alloys can be compared to the $d\mu/dx$ values measured experimentally. The results obtained for $3d$ and $4d$ impurities

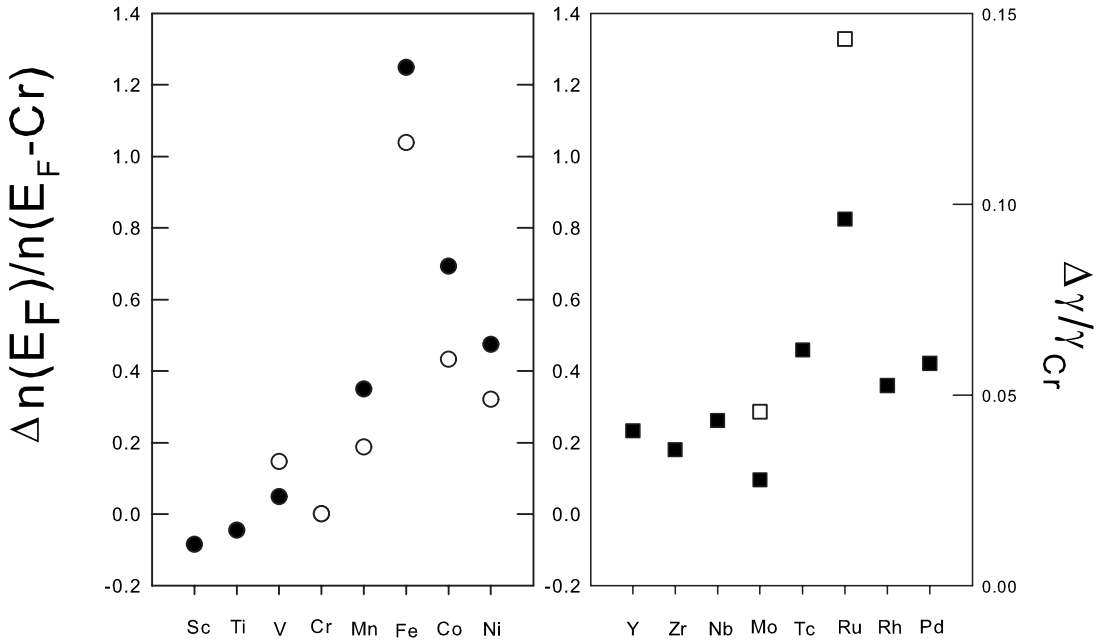

FIG. 5. Relative change in calculated density of states at the Fermi energy $\Delta n(E_F)/n(E_F)$ (filled symbols) and experimentally measured electronic specific heat $\Delta\gamma/\gamma$ (open symbols) of Cr-X alloys; X=Sc to Ni and Y to Pd. The experimental values have been taken from Refs. 2 and 21–24

are shown in Fig. 6 along with the experimental data available. It is satisfying to note that the calculated results reasonably reproduce the trend observed experimentally.[2]

D. Hyperfine fields

In addition to the thermodynamic properties discussed above, we have calculated the hyperfine fields (HF) of 3d and 4d impurities in Cr host to examine their magnetic behavior at a microscopic level. The hyperfine field generally has contributions from dipolar, orbital, and Fermi contact interactions. For the cases studied here, because of the cubic point symmetry, the orbital and dipolar fields are negligibly small. The dominant contribution to HF thus arises from Fermi contact interaction, which depends on the s-electron spin density at the nuclear site $n^s(0)$. The HF values were calculated using the scalar relativistic formula,[36]

$$B_{hf} = (8\pi/3)\mu_B m_{av};$$

$$m_{av} = \int^{E_F} dE[F_0^+(E)n_0^+(E) - F_0^-(E)n_0^-(E)], \quad (3)$$

implemented within the WIEN2K program.[7] The results are displayed in Fig. 7 and summarized in Table III. Also shown are the results for the core and valence contributions (B_{hf}^{core} and B_{hf}^{val}) to the HF values. For the 3d impurities, the magnitudes of the core and valence hyperfine fields B_{hf}^{core} and B_{hf}^{val}, opposite in sign, increase from Sc to Mn and then decrease for Fe, Co, and Ni. The two contributions cancel in between Mn-Fe, resulting in a change of sign for the total hyperfine field B_{hf}^{tot}. The variation of B_{hf}^{tot} is similar to the trend observed for the impurity local moment (see Fig. 6). For the 4d impurities also the B_{hf}^{tot} shows a sign change near

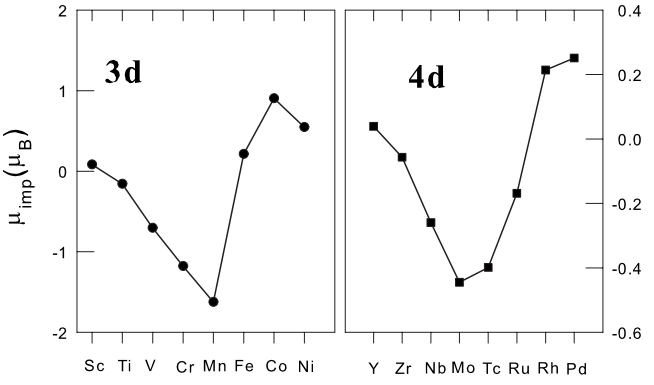

FIG. 6. The magnetic moment of 3d and 4d impurities in Cr host.

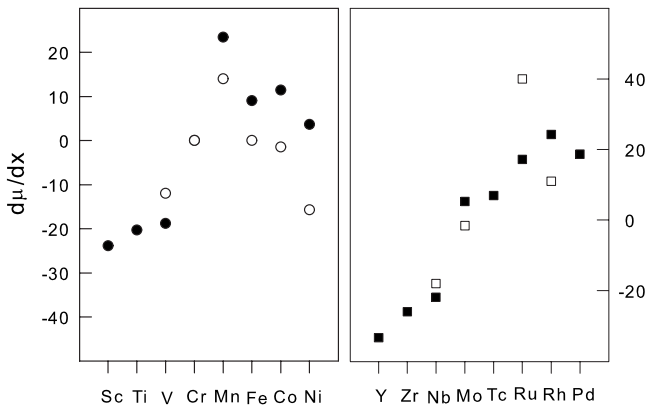

FIG. 7. Moment change per impurity atom ΔM for dilute Cr-X alloys, X=Sc-Ni, and Y-Pd. Filled symbols: Present calculations; open symbols: Experimental data taken from Ref. 2.

TABLE III. Summary of the calculated magnetic hyperfine fields of 3*d* and 4*d* impurities in antiferromagnetic Cr host. B_{hf}^{tot} (kG) denotes the total hyperfine field, while B_{hf}^{core} (kG) and B_{hf}^{val} (kG) are the core and valence contributions, respectively. Also shown are the total hyperfine field for the nearest neighbor Cr atom. The last column shows the experimental values of total impurity hyperfine field taken from Refs. 38–40.

Impurity	B_{hf}^{tot}	B_{hf}^{core}	B_{hf}^{val}	B_{hf}^{tot} (Cr-1nn)	HF_{imp} (exp)
Sc	−23.51	−3.18	−20.33	14.17	
Ti	−15.24	20.40	−30.64	16.64	
V	2.66	102.19	−99.53	−17.07	
Cr	23.71	194.46	−170.75	23.71	
Mn	41.10	229.22	−188.12	27.89	
Fe	−40.67	−23.97	−16.70	20.58	36.0[a]
Co	−76.99	−108.76	31.77	25.88	
Ni	−57.38	−67.82	−10.44	21.7	
Y	88.80	−5.4	94.2	8.43	
Zr	50.67	0.95	49.72	10.40	
Nb	40.05	10.41	30.64	13.15	
Mo	33.46	22.87	10.59	16.54	47.0[b]
Tc	20.64	22.18	−1.55	17.39	
Ru	−20.60	−1.91	−18.69	18.46	0.0[c]
Rh	−72.25	−30.20	−42.05	27.55	65.0[d]
Pd	−112.31	−60.26	−52.04	33.07	

[a]Reference 26 and 28.
[b]Reference 38.
[c]Reference 39.
[d]Reference 40.

Ru, which is consistent with the feature observed for the impurity moment displayed in Fig. 6. The calculated magnetic hyperfine fields can be compared to experimental values available in literature. Unlike the ferromagnetic hosts Fe, Co, and Ni, measurements in antiferromagnetic Cr metal have been limited to a few impurities like Fe, Cu, Mo, Ru, Rh, Cd, Sn, and Ta.[26–28,38–41] The B_{hf} values measured for Fe, Mo, Ru, and Rh are listed in Table III It can be noticed that the total hyperfine field calculated for these impurities closely agree with experimental results.[26–28,38–40] In particular, we like to point out that the hyperfine field of Fe in Cr B_{hf}=−40.7 kG, obtained from our 3×3×3 calculations ($Cr_{53}Fe$) shows excellent agreement with the experimental data as compared to the value 71.6 kG obtained for $Cr_{15}Fe$ by Hashemifar *et al.*[4] This discrepancy once again suggests that impurity-impurity interaction plays a significant role on the magnetic behavior of Cr-*X* alloys—a point we shall discuss later.

Next we discuss the individual contributions to the hyperfine fields, i.e., the core and valence contributions B_{hf}^{core} and B_{hf}^{val}, which are listed in Table III. For magnetic impurities B_{hf}^{core} is large because of exchange interaction of the polarized *d* shell with the core *s* orbitals. In general, $B_{\mathrm{hf}}^{\mathrm{core}}$ scales with the local moment of the impurity and has the opposite sign. The valence contributions to the hyperfine fields B_{hf}^{val} are more complicated. It has two major contributions: (i) from the polarization of outer *s* orbitals of the impurity by its own local moment and (ii) polarization of valence electrons due to the magnetic moments of the neighboring host atoms. The later, known as the transferred field, is usually proportional to the magnetic moments of the surrounding host atoms and positive with respect to its direction. Figure 8 displays the variation of B_{hf}^{tot}, B_{hf}^{core}, and B_{hf}^{val} with respect to the impurity local moment of 3*d* and 4*d* impurities in Cr. In the case of 3*d* impurities, the HF values scale with the impurity local moment, yielding hyperfine coupling constants: A_{core} =−140 kG/μ_B, A_{val}=+90 kG/μ_B, and A_{tot}=−50 kG/μ_B. These values are comparable to the results reported for 3*d* impurities in ferromagnetic Fe, Co, and Ni hosts.[18,30,34,36] The corresponding hyperfine coupling constants for the 4*d* impurities come out to be: A_{core}

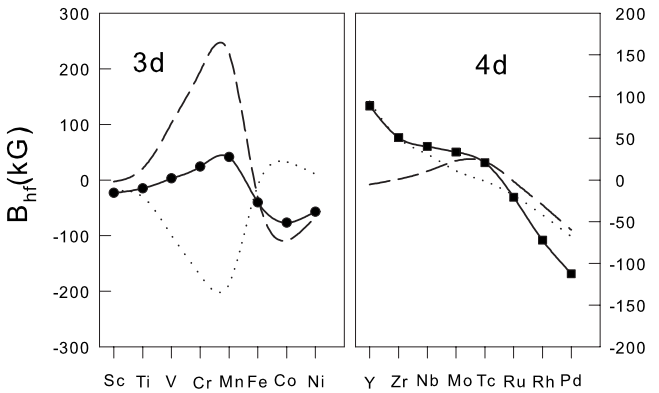

FIG. 8. Magnetic hyperfine fields of 3*d* and 4*d* impurities in Cr host. Filled symbols and solid line represent the total hyperfine field B_{hf}^{tot}. The dotted and dashed lines represent the core and valence contributions, respectively. The open symbols are experimental data taken from Refs. 26–28 and 34–37

$=-114$ kG/μ_B, $A_{\text{val}}=-97$ kG/μ_B, and $A_{\text{tot}}=-197$ kG/μ_B. It must be mentioned that the data for Y and Zr deviates from the above proportionality probably because of higher valence contribution. Looking at the results shown in Fig. 8, the observed proportionality between B_{hf} and the impurity moments suggests that the hyperfine fields of $3d$ and $4d$ impurities in Cr is dominated by the local contributions with relatively weak transferred field from the neighboring Cr atoms.

For further analysis of the different contributions to the total hyperfine field at the impurity site, we write

$$B_{hf}^{\text{tot}} = aM_{\text{loc}} + bM_{\text{host}} + c\sum_{i=NN} \delta M_i, \tag{4}$$

where the first term represents the local hyperfine field of the impurity, being the sum of the local core and valence contributions, which are proportional to the local moment of the impurity. The second and third terms represent the transferred hyperfine field consisting of a constant contribution bM_{host} and a correction $c\Sigma_{i=NN}\delta M_i$ due to impurity induced perturbations in the magnetic moments of neighboring host atoms. By using the calculated values for $\Delta M = \text{sum}_{i=1\ldots7}\delta M_i$, the B_{hf}^{tot} shown in Table II could be fitted reasonably well with the constants a, b, and c as

$$a \approx -50 \text{ kG}/\mu_B,$$

$$b \approx -20 \text{ kG}/\mu_B,$$

and

$$c \approx -10 \text{ kG}/\mu_B$$

for $3d$ impurities. The corresponding values for the $4d$ impurities were found to be

$$a \approx -200 \text{ kG}/\mu_B,$$

$$b \approx -38 \text{ kG}/\mu_B,$$

and

$$c \approx -18 \text{ kG}/\mu_B.$$

The above analysis, although does not accurately reproduce the HF values for all of the cases studied, it shows the trend that the transferred component is relatively weak compared to the local contribution, as shown in Fig. 9.

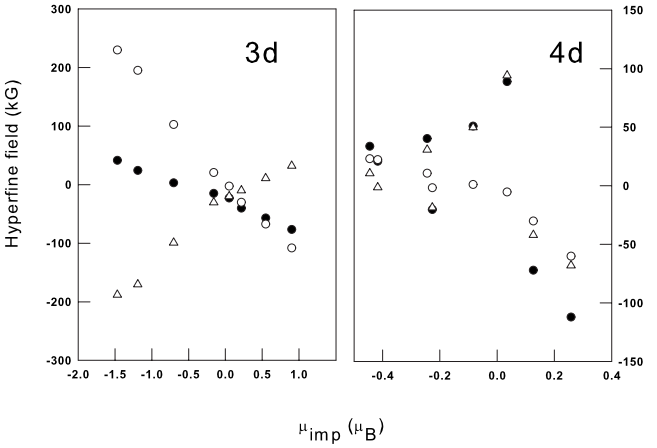

FIG. 9. Variation of hyperfine fields as a function of impurity local moment for $3d$ and $4d$ impurities in Cr host. ●: B_{hf}^{tot}; ○: core hyperfine field and △: valence contribution to HF.

E. Concentration dependence

Finally we come to discuss the influence of impurity concentration on the magnetic moment, as well as hyperfine fields. For this, we compare the results calculated for $Cr_{53}X$ ($3\times3\times3$ supercell) and $Cr_{15}X$ ($2\times2\times2$ supercell). The two supercells are equivalent to Cr-X alloys with concentration of X being 0.0185 and 0.0625, respectively. For the $2\times2\times2$ supercell calculations, we used the lattice parameters shown in Table I, scaled by a factor 2/3 to account for the difference in supercell size. The Brillouin zone integration in this case was done with a finer k-mesh consisting of 84 k-points in the irreducible zone, as compared to 56 k-points used by Hashemifar *et al.*[4] The calculated impurity magnetic moments and the hyperfine field values are listed in Table IV.

The moment values obtained from our $2\times2\times2$ supercell calculations closely agree with the results reported by Antropov *et al.*[3] and Hashemifar *et al.*[4] It should also be mentioned that apart from the minimum energy spin configuration mentioned in Table IV, we also obtain a ferromagnetic solution for Mn with a moment of $2.04\mu_B$ with slightly higher energy (≈1 mRy). Similarly, for Fe we get an antiferromagnetic solution with a moment of $1.94\mu_B$ with total energy 4 mRy higher than the ferromagnetic solution. These observations are consistent with the results reported earlier.[3,4] Comparing the results of $Cr_{15}X$ (Table IV) with the values calculated for $Cr_{53}X$ (Tables II and III), it can be clearly noticed that the magnitude of impurity local moment and the

TABLE IV. Magnetic moments and hyperfine fields calculated for $Cr_{15}X$ (X=Sc-Ni and Y–Pd). μ_{imp}: Impurity magnetic moment in μ_B; B_{hf}^{tot}: Total magnetic hyperfine field in kG.

	Sc	Ti	V	Cr	Mn	Fe	Co	Ni
μ_{imp}	+0.04	−0.15	−0.57	+1.18	−1.60	+0.59	+1.08	+0.64
B_{hf}^{tot}	−15.7	−1.35	+3.66	+23.51	+35.92	−68.51	−100.85	−80.43
	Y	Zr	Nb	Mo	Tc	Ru	Rh	Pd
μ_{imp}	0.023	−0.057	−0.260	−0.432	−0.399	−0.169	+0.213	+0.251
B_{hf}^{tot}	86.80	+34.69	+28.71	+13.60	−6.86	−38.88	−88.62	−93.82

related hyperfine field is substantially different for V, Mn, Fe, Co, and Ni. For 4*d* impurities, however, the size of the supercell did not have much influence on the magnetic properties. The results thus demonstrate that impurity-impurity interaction plays an important role on the local magnetic properties of 3*d* impurities in Cr host, particularly, for the cases of Mn, Fe, and Co.

The differences in the magnetic behavior between the present work and the earlier ones,[3,4] especially for 3*d* impurities, can also be due to small variations in the lattice constants used. Cottenier *et al.* have earlier shown that within GGA formalism, the magnetic moment of Cr significantly changes with lattice constant, decreasing from $1.19\mu_B$ at the equilibrium value of the lattice constant $a=2.876$ Å to $0.68\mu_B$ at $a=2.81$ Å. The later being in agreement with the experimental result $0.67\mu_B$/Cr.[11] We therefore calculated the magnetic moment and hyperfine fields for a few cases of 3*d* impurities V, Cr, Mn, Fe, Co, and Ni using a $3\times3\times3$ supercell with lattice parameter $a=2.81$ Å but keeping all other parameters: R_{MT}, $k_{\max}$, $G_{\max}$, and *k*-mesh size same as in the calculations discussed before. The magnetic moment and hyperfine fields from these calculations came out to be μ_{imp}, $B_{hf}=(-0.30\mu_B, 1.9$ kG), $(-0.69\mu_B, 12.3$ kG), $(-0.82\mu_B, 18.4$ kG), $(0.44\mu_B, -46$ kG), $(0.95\mu_B, -82$ kG), and $(0.27\mu_B, -46$ kG) for, Cr, Mn, Fe, Co, and Ni, respectively. The differences between the present and earlier results, although is reduced by decreasing the lattice constant, still remains significantly large, especially for Mn, Fe, Co, and Ni. Furthermore, considering that the calculated equilibrium lattice constant of pure Cr closely agrees with the experimental value (see Table I), and the impurity concentration used for our studies is small (<2 at %), it is hard to imagine a physical reason for such a large reduction of the unit cell parameter. We therefore believe that the discrepancies mentioned above is mainly from impurity-impurity interaction.

In summary, using full-potential linearized augmented plane wave (FLAPW) method based on the density function theory (DFT), we have made detailed *ab initio* calculations for the magnetic properties of dilute Cr-*X* alloys with 3*d* and 4*d* transition metals. The calculations performed for nonmagnetic, as well as antiferromagnetic cases, yield important information regarding both local and global properties of dilute Cr alloys. By analyzing the nonmagnetic density of states (DOS) within Stoner model, we find that the condition for local moment formation is satisfied only for Fe, Co, and Ni, while the moment of Mn is predicted to be unstable. The magnetic moments for all other cases appear to be induced by Cr-host magnetism. The calculations, systematically carried out for all of the elements in 3*d* (Sc–Ni) and 4*d* (Y–Pd) series, have enabled us to establish the trends for the impurity local magnetic moments and hyperfine fields in Cr host. The trends observed for antiferromagnetic Cr are found to be remarkably similar to the ones reported for ferromagnetic hosts Fe, Co, and Ni. Furthermore, our results for the total alloy moment arising from induced host perturbations show satisfactory agreement with available experimental data. In addition to the local properties mentioned above, our results for the impurity induced changes in total density of states at Fermi energy reproduce the trend observed for the specific heat of Cr alloys. By calculating the magnetic properties for unit cells with different impurity concentrations, we have illustrated the influence of impurity-impurity interaction on the magnetic behavior of the impurity atoms. The results presented in this work provide a basis for comprehensive and improved understanding of the local magnetic properties of 3*d* and 4*d* impurities in Cr host, as well as macroscopic properties such as changes in total magnetization and specific heat of dilute Cr alloys. They are also useful toward a common understanding of magnetic hyperfine fields of transition metal impurities in ferromagnetic and antiferromagnetic hosts.

ACKNOWLEDGMENTS

We thank Stefaan Cottenier for many enlightening discussions. We also thank S. K. Srivastava for discussion and technical help.

*mishra@tifr.res.in

[1] E. Fawcett, Rev. Mod. Phys. **60**, 209 (1988).
[2] E. Fawcett, H. L. Albetrs, V. Yu Galkin, R. R. Noakes, and J. V. Yakhami, Rev. Mod. Phys. **66**, 25 (1994).
[3] V. P. Antropov, V. I. Anisimov, A. I. Liechtenstein, and A. V. Postnikov, Phys. Rev. B **37**, 5603 (1988).
[4] S. J. Hashemifar, N. Ghaderi, S. Sirousi, and H. Akbarzadeh, Phys. Rev. B **73**, 165111 (2006).
[5] P. Hohenberg and W. Kohn, Phys. Rev. **136**, B864 (1964).
[6] W. Kohn and L. J. Sham, Phys. Rev. **140**, A1133 (1965).
[7] P. Blaha, K. Schwarz, G. Madsen, D. Kvasnicka, and J. Luitz, *WIEN2k an Augmented Plane Wave Plus Local Orbitals Programm for Calculating Crystal Properties* (Karlheinz Schwarz, Technische Universitat Wien, Austria, 1999).
[8] S. Cottenier, *Density Functional Theory and the Family of (L)APW-Methods: A Step-By-Step Introduction* (Instituut voor Kern- en Stralingsfysica, K. U. Leuven, Belgium, 2002).
[9] J. P. Perdew, K. Burke, and M. Ernzerhof, Phys. Rev. Lett. **77**, 3865 (1996).
[10] F. Birch, Phys. Rev. **71**, 809 (1947); F. D. Murnaghan, *Finite Deformation of an Elastic Solid* (Wiley, New York, 1951).
[11] S. Cottenier, B. De Vries, J. Meersschaut, and M. Rots, J. Phys.: Condens. Matter **14**, 3275 (2002).
[12] V. L. Moruzzi, J. F. Janak, and A. R. Williams, *Calculated Electronic Properties of Metals* (Pergamon, New York, 1978).
[13] T. Beuerle, K. Hummler, C. Elsässer, and M. Fähnle, Phys. Rev. B **49**, 8802 (1994).
[14] K. Willenborg, R. Zeller, and P. H. Dederichs, Europhys. Lett. **18**, 263 (1992).
[15] V. L. Moruzzi and P. M. Marcus, Phys. Rev. B **46**, 3171 (1992).
[16] R. Hafner, D. Spisak, R. Lorenz, and J. Hafner, Phys. Rev. B **65**, 184432 (2002).
[17] J. Chen, D. Singh, and H. Krakauer, Phys. Rev. B **38**, 12834 (1988).

[18] B. Drittler, N. Stefanou, S. Blügel, R. Zeller, and P. H. Dederichs, Phys. Rev. B **40**, 8203 (1989).
[19] W. L. McMillan, Phys. Rev. **167**, 331 (1968).
[20] F. Sacchetti, J. Phys. F: Met. Phys. **10**, 801 (1980).
[21] F. Heiniger, E. Bucher, and J. Muller, Phys. Kondens. Mater. **5**, 243 (1966).
[22] N. P. Baum and K. Schröder, Phys. Rev. B **3**, 3847 (1971).
[23] J. Takeuchi, H. Sasakura, and Y. Masuda, J. Phys. Soc. Jpn. **49**, 508 (1980).
[24] V. Yu. Galkin, W. A. Ortiz, R. Black, J. Diederichs, S. Spagna, and E. Fawcett, Physica B (Amsterdam) **339**, 137 (2003).
[25] P. Hill, N. Ali, A. J. A. De Oliveria, W. A. Ortiz, P. C. de Camargo, and E. Fawcett, J. Phys.: Condens. Matter **6**, 1761 (1994).
[26] M. Shiga and N. Nakamura, J. Phys. Soc. Jpn. **49**, 528 (1980).
[27] S. M. Dubiel and W. Zinn, J. Magn. Magn. Mater. **23**, 214 (1981).
[28] D. Riegel, L. Büermann, K. D. Gross, M. Luszik-Bhadra, and S. N. Mishra, Phys. Rev. Lett. **62**, 316 (1989).
[29] V. Yu. Galkin, N. Ali, E. Fawcett, and P. C. de Camargo, J. Phys.: Condens. Matter **10**, 4901.(1998).
[30] H. Akai, M. Akai, and J. Kanamori, J. Phys. Soc. Jpn. **54**, 4257 (1985).
[31] S. Cottenier and H. Haas, Phys. Rev. B **62**, 461 (2000).
[32] H. Haas and S. Cottenier, J. Magn. Magn. Mater. **226-230**, 1035 (2001).
[33] S. Cottenier and H. Haas, Hyperfine Interact. **133**, 239 (2001).
[34] V. S. Stepanyuk, R. Zeller, P. H. Dederichs, and I. Mertig, Phys. Rev. B **49**, 5157 (1994).
[35] C. Paduani, J. Magn. Magn. Mater. **278**, 76 (2004).
[36] S. Blügel, H. Akai, R. Zeller, and P. H. Dederichs, Phys. Rev. B **35**, 3271 (1987).
[37] R. Zeller, J. Phys. F: Met. Phys. **17**, 2123 (1987).
[38] S. N. Mishra, Solid State Commun. **146**, 279 (2008).
[39] G. N. Rao, P. Peretto, R. Venegas, L. Trabut, and S. Choulet, Phys. Lett. **75A**, 403 (1980).
[40] G. N. Rao, Hyperfine Interact. **26**, 1119 (1985).
[41] S. K. Srivastava and S. N. Mishra, J. Phys.: Condens. Matter **20**, 015214 (2008).